

# Hyperactivation of HUSH complex function by Charcot–Marie–Tooth disease mutation in *MORC2*

Iva A Tchasovnikarova<sup>1,2,6</sup> , Richard T Timms<sup>1,6</sup>, Christopher H Douse<sup>3</sup>, Rhys C Roberts<sup>4</sup> , Gordon Dougan<sup>5</sup>, Robert E Kingston<sup>2</sup>, Yorgo Modis<sup>3</sup>  & Paul J Lehner<sup>1</sup>

**Dominant mutations in the *MORC2* gene have recently been shown to cause axonal Charcot–Marie–Tooth (CMT) disease, but the cellular function of *MORC2* is poorly understood. Here, through a genome-wide CRISPR–Cas9-mediated forward genetic screen, we identified *MORC2* as an essential gene required for epigenetic silencing by the HUSH complex. HUSH recruits *MORC2* to target sites in heterochromatin. We exploited a new method, differential viral accessibility (DIVA), to show that loss of *MORC2* results in chromatin decompaction at these target loci, which is concomitant with a loss of H3K9me3 deposition and transcriptional derepression. The ATPase activity of *MORC2* is critical for HUSH-mediated silencing, and the most common alteration affecting the ATPase domain in CMT patients (p.Arg252Trp) hyperactivates HUSH-mediated repression in neuronal cells. These data define a critical role for *MORC2* in epigenetic silencing by the HUSH complex and provide a mechanistic basis underpinning the role of *MORC2* mutations in CMT disease.**

Chromatin has historically been considered to exist in one of two distinct states: euchromatin or heterochromatin. Euchromatin is generally thought to be gene rich, transcriptionally active and associated with an open and accessible conformation, whereas heterochromatin is comparatively gene poor, highly condensed and refractory to the transcription machinery<sup>1</sup>. Heterochromatin has traditionally been considered to occur in two distinct types: that marked with Lys27-trimethylated histone H3 (H3K27me3), which is dynamically deposited during development<sup>2</sup>, and that marked with Lys9-trimethylated H3 (H3K9me3), which is typically found at repeat-rich regions<sup>3</sup>.

A remarkable property of H3K9me3-marked heterochromatin is that it can ‘spread’ along the arm of a chromosome, thus resulting in the epigenetic repression of an active gene in the vicinity of a heterochromatic domain<sup>4</sup>. This phenomenon gives rise to chromosomal position effects, a term referring to differences in expression when an identical gene is positioned at different sites in the genome<sup>5,6</sup>. We have previously exploited the near-haploid KBM7 cell line<sup>7,8</sup> to identify genes required for position-effect variegation in human cells<sup>9</sup>. By isolating a population of cells that displayed epigenetic repression of an integrated green fluorescent protein (GFP) reporter construct and screening for mutants in which this repression was alleviated, we identified four genes encoding proteins essential for transgene repression: the histone lysine methyltransferase SETDB1 (ref. 10) and the human silencing hub (HUSH) complex subunits TASOR, MPP8 and Periphilin<sup>9</sup>. Through the chromodomain of MPP8 (ref. 11), HUSH preferentially localizes to genomic loci rich in the repressive histone modification H3K9me3. HUSH-mediated recruitment of the

methyltransferase SETDB1 to these sites results in the ‘writing’ of additional H3K9me3, thereby mediating the spreading of heterochromatin across incoming transgenes<sup>9</sup>. The HUSH complex also plays a critical role in endogenous heterochromatin maintenance, as deletion of HUSH subunits results in decreased H3K9me3 at hundreds of genomic loci<sup>9</sup> and in early embryonic lethality in mice<sup>12,13</sup>.

HUSH-mediated silencing is achieved through the reading and writing of H3K9me3. However, to understand how the deposition of this modification ultimately results in epigenetic repression, knowledge of the full complement of HUSH components is essential. Although our original haploid screen identified the core HUSH complex members and SETDB1, our recent examination of the efficacy of the haploid gene-trap approach has suggested that such screens are unlikely to achieve saturation<sup>14</sup>. HUSH-mediated silencing may therefore require additional factors not identified by the original gene-trap screen, and, in support of this idea, we recently identified ATF7IP as an additional factor required for HUSH-mediated repression, by using a proteomic approach<sup>15</sup>.

With the aim of identifying additional genes required for transgene silencing by the HUSH complex, we carried out a genome-wide forward genetic screen using CRISPR–Cas9 technology<sup>16,17</sup>. The CRISPR screen highlighted one additional gene as being critical for HUSH-mediated repression: microchidia CW-type zinc-finger 2 (*MORC2*). Here, we found that HUSH recruits *MORC2* to heterochromatic sites, where its ATPase activity is required to mediate transgene silencing. Loss of *MORC2* results in chromatin decompaction at HUSH-target loci, concomitant with a loss of H3K9me3 and transcriptional

<sup>1</sup>Department of Medicine, Cambridge Institute for Medical Research, Cambridge, UK. <sup>2</sup>Department of Molecular Biology, Massachusetts General Hospital, and Department of Genetics, Harvard Medical School, Boston, Massachusetts, USA. <sup>3</sup>Department of Medicine, University of Cambridge, MRC Laboratory of Molecular Biology, Cambridge, UK. <sup>4</sup>Department of Clinical Neurosciences, Cambridge Institute for Medical Research, Cambridge, UK. <sup>5</sup>Wellcome Trust Sanger Institute, Hinxton, UK. <sup>6</sup>These authors contributed equally to the work. Correspondence should be addressed to P.J.L. ([pjl30@cam.ac.uk](mailto:pjl30@cam.ac.uk)).

Received 15 January; accepted 26 April; published online 5 June 2017; doi:10.1038/ng.3878

derepression. Alterations in residues in the ATPase domain of MORC2 have recently been implicated in CMT disease, one of the most frequently inherited neurological disorders. We found that the most common of these alterations (p.Arg252Trp) results in hyperactivation of HUSH-mediated silencing in neuronal cells. Overall, this study identifies a critical role for MORC2 in HUSH-mediated repression and provides further insight into the mechanisms underlying HUSH complex function in health and disease.

## RESULTS

### MORC2 is essential for HUSH-mediated silencing

The rapid emergence of CRISPR–Cas9-mediated genome editing technologies allowed us to reevaluate the set of genes required for HUSH-mediated transgene silencing (Fig. 1a). The Cas9 nuclease was expressed in the same population of GFP<sup>dim</sup> KBM7 cells stably expressing epigenetically repressed transgenes that we have used previously<sup>9</sup>, and genome-wide CRISPR-mediated mutagenesis was performed with the GeCKO v2 single guide RNA (sgRNA) library<sup>18</sup>. Two rounds of fluorescence-activated cell sorting (FACS) were used to enrich for GFP<sup>bright</sup> cells in which epigenetic repression of the GFP reporter transgene was relieved (Fig. 1b), and sgRNA abundance in the selected GFP<sup>bright</sup> cells compared with the unselected library of

mutagenized cells was quantified by Illumina sequencing (Fig. 1c and Supplementary Fig. 1a).

Five genes are known to encode proteins critical for HUSH-mediated transgene repression: the three HUSH complex subunits TASOR, MPP8 and Periphilin<sup>9</sup>, plus the histone methyltransferase SETDB1 (ref. 9) and its accessory factor ATF7IP<sup>15</sup>. Three of these positive controls, MPP8, SETDB1 and ATF7IP, were successfully identified by the CRISPR screen; however, TASOR and Periphilin were not significantly enriched, thus suggesting that the screen did not reach saturation (Fig. 1c and Supplementary Fig. 1a). Through individual CRISPR–Cas9-mediated gene disruption experiments, we assessed potential roles for the other most significantly enriched genes in transgene silencing (Supplementary Fig. 1b). The results revealed an essential role for one additional gene, MORC2, a finding that we corroborated in an independent HeLa-cell clone bearing a HUSH-repressed GFP reporter construct<sup>9</sup> (Fig. 1d,e). With the exception of SEL1L, which mediates the degradation of the GFP reporter at the protein level<sup>14</sup>, we were unable to validate any of the additional candidate genes (Supplementary Fig. 1b). Therefore, the genome-wide CRISPR screen identified a single novel gene, MORC2, encoding a bona fide factor required for HUSH-mediated transgene repression.

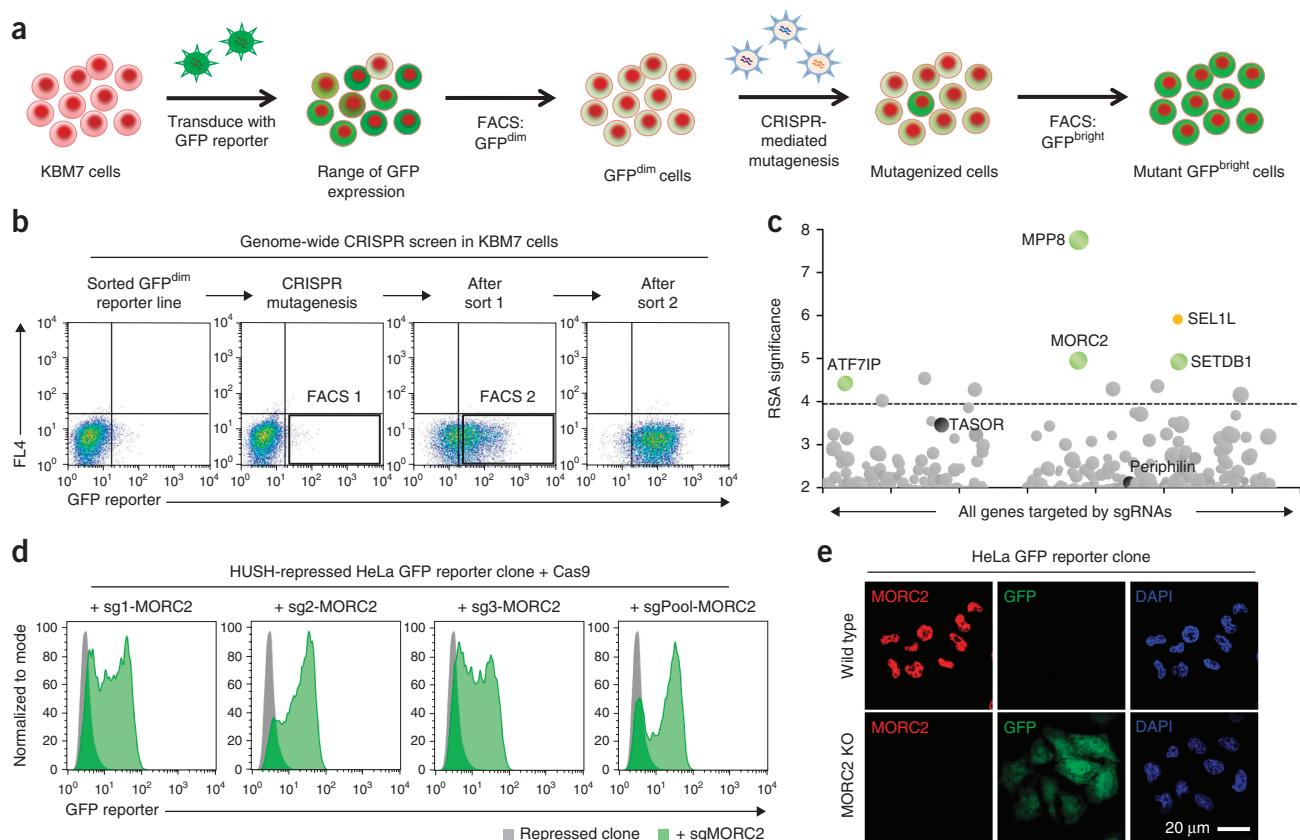


**Figure 1** A genome-wide CRISPR–Cas9-mediated forward genetic screen identifies an essential role for MORC2 in transgene silencing by the HUSH complex. **(a,b)** A genome-wide CRISPR screen to identify genes required for transgene silencing. **(a)** Cas9 was expressed in a population of GFP<sup>dim</sup> KBM7 cells bearing epigenetically repressed transgenes, and genome-wide mutagenesis was carried out with the GeCKO v2 sgRNA library. **(b)** Mutant GFP<sup>bright</sup> cells harboring gene-disruption events that prevented reporter repression were isolated through two sequential rounds of FACS. Black boxes indicate approximate sorting gates. **(c)** Bubble plot illustrating the hits from the screen. All genes targeted by sgRNAs are arranged alphabetically by name along the x axis, and statistical significance, as determined by the RSA algorithm, is plotted on the y axis. Bubble size is proportional to the number of active sgRNAs for each gene. Colored bubbles represent validated hits; the HUSH complex subunits TASOR and Periphilin (black) did not reach statistical significance, whereas SEL1L (orange) is involved in the degradation of the GFP-fusion protein<sup>14</sup>. A fully annotated plot is provided in **Supplementary Figure 1**. **(d,e)** MORC2 is required for transgene silencing by the HUSH complex in HeLa cells. CRISPR–Cas9-mediated disruption of MORC2 results in derepression of a HUSH-repressed reporter, as measured by flow cytometry **(d)** or immunofluorescence microscopy **(e)**. The ‘sg’ prefix denotes sgRNAs. KO, knockout.

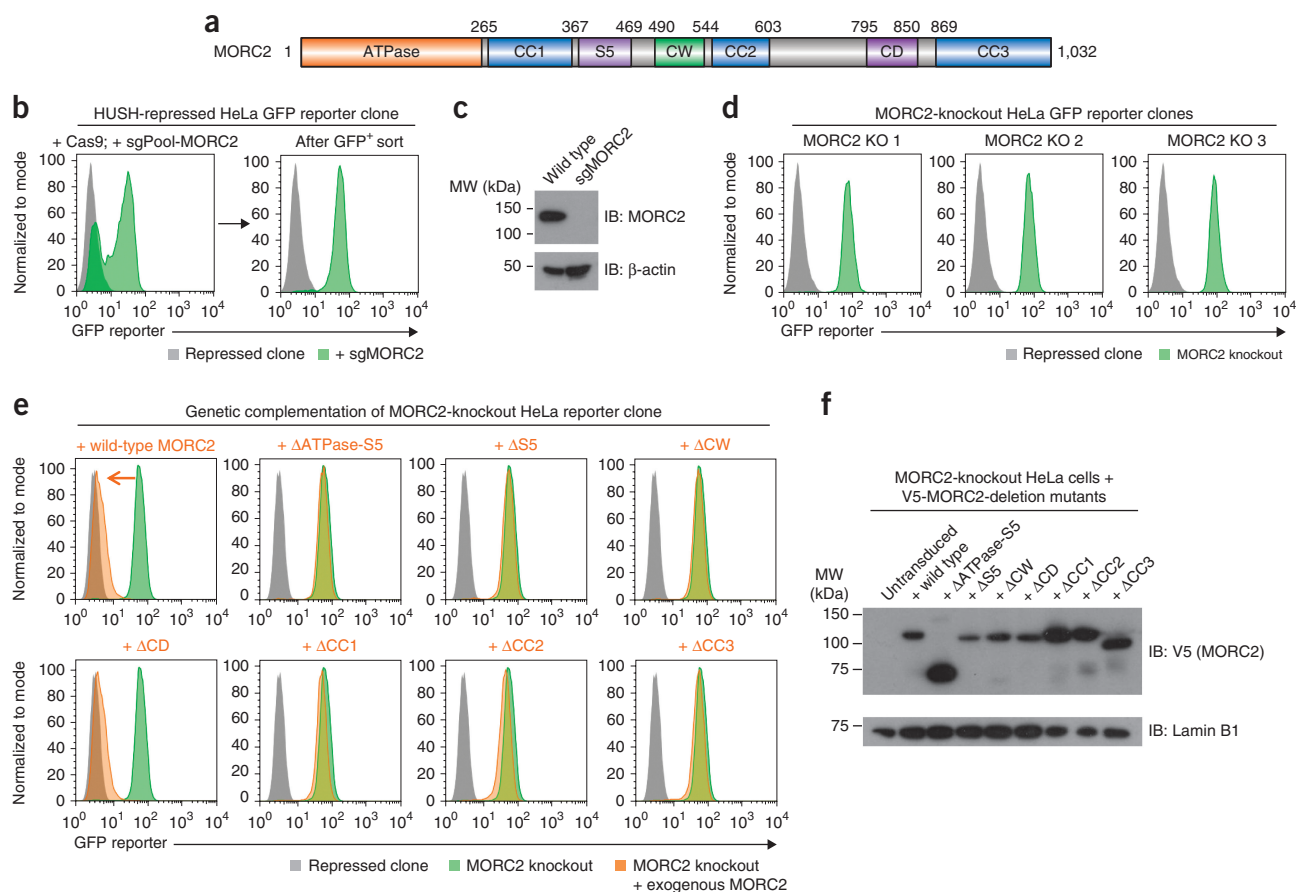


**Figure 2** The ATPase, CW and coiled-coil domains of MORC2 are required for HUSH complex function. **(a)** Schematic representation of the domain structure of MORC2. (CC, predicted coiled coil; S5, ribosomal S5-like domain; CW, CW-type zinc-finger; CD, chromo-like domain). **(b–d)** Generation and validation of MORC2-knockout HeLa cells. A HeLa reporter clone bearing a HUSH-repressed GFP reporter was transfected with a pool of plasmids to express Cas9 and three sgRNAs targeting MORC2. **(b)** Cells in which the MORC2 gene was disrupted became GFP positive (GFP<sup>+</sup>), owing to derepression of the GFP reporter, and were isolated with FACS. **(c)** The sorted GFP<sup>+</sup> population no longer expressed MORC2 protein, as assessed by immunoblotting (IB). MW, molecular weight. **(d)** MORC2-knockout single-cell clones were then isolated from the GFP<sup>+</sup>-sorted population. **(e,f)** Assessing the domains required for MORC2 function through the genetic complementation of MORC2-knockout cells. **(e)** Expression of wild-type MORC2 or a MORC2 mutant lacking the chromodomain (ΔCD) in MORC2-knockout cells resulted in repression of the GFP reporter transgene. In contrast, MORC2 variants lacking the ATPase, S5, CW or coiled-coil domains were nonfunctional and did not rescue HUSH-mediated repression. **(f)** Immunoblot validation of expression of the MORC2-deletion mutants. All MORC2 variants were expressed with an N-terminal V5 epitope tag followed by an exogenous SV40 nuclear localization signal; detailed sequence information on the composition of the mutants is provided in **Supplementary Table 1**.

### Essential roles of MORC2 protein domains in HUSH function

MORC2 is one of four MORC family proteins in humans (MORC1–4)<sup>19</sup>. Although little is known about their functional role in human cells, MORC family proteins have been implicated in epigenetic silencing in plants, worms and mice<sup>20,21</sup>. *MORC2* encodes a protein containing a GHKL-type ATPase, comprising the N-terminal ATPase domain plus an associated ribosomal protein S5-like domain, which is followed by two putative histone-binding modules: a CW-type zinc-finger and a chromo-like domain (Fig. 2a). To assess which of these domains are required for the function of MORC2 in HUSH-mediated repression, we performed a series of genetic complementation experiments in a MORC2-knockout HeLa clone (Fig. 2b–d and **Supplementary Table 1**). Whereas exogenous expression of full-length MORC2 or a MORC2 mutant lacking the chromo-like domain resulted in repression of the GFP reporter, deletion of both ATPase domains, the S5-like domain alone or the CW-type zinc-finger abolished MORC2 activity (Fig. 2e,f). Sequence analysis also predicted the presence of three coiled-coil domains (denoted CC1, CC2 and CC3) (Fig. 2a); deletion of any one of these domains also abrogated

MORC2 function (Fig. 2e,f). Thus, the MORC2 ATPase domain, CW-type zinc-finger and coiled-coil domains, but not the chromo-like domain, appeared to be critical for HUSH-mediated epigenetic repression, with the caveat that although these mutant proteins were expressed in cells (Fig. 2f), we are unable to verify that they were correctly folded.

### MORC2 interacts with the HUSH complex

The genetic association between *MORC2* and the HUSH complex suggested that MORC2 might physically interact with HUSH subunits. We were readily able to detect an interaction between V5 epitope-tagged MORC2 immunoprecipitated from HeLa nuclei and the HUSH subunits TASOR and MPP8 (Fig. 3a). To delineate the region of MORC2 responsible for this interaction, we repeated this assay with a series of V5-tagged N- and C-terminal-truncation mutants of MORC2 (**Supplementary Table 1**). The results suggested that the second coiled-coil domain (CC2) of MORC2 (residues 548–603) was likely to be essential for this interaction (**Supplementary Fig. 2a–c**). The interaction between MORC2 and HUSH subunits also occurred

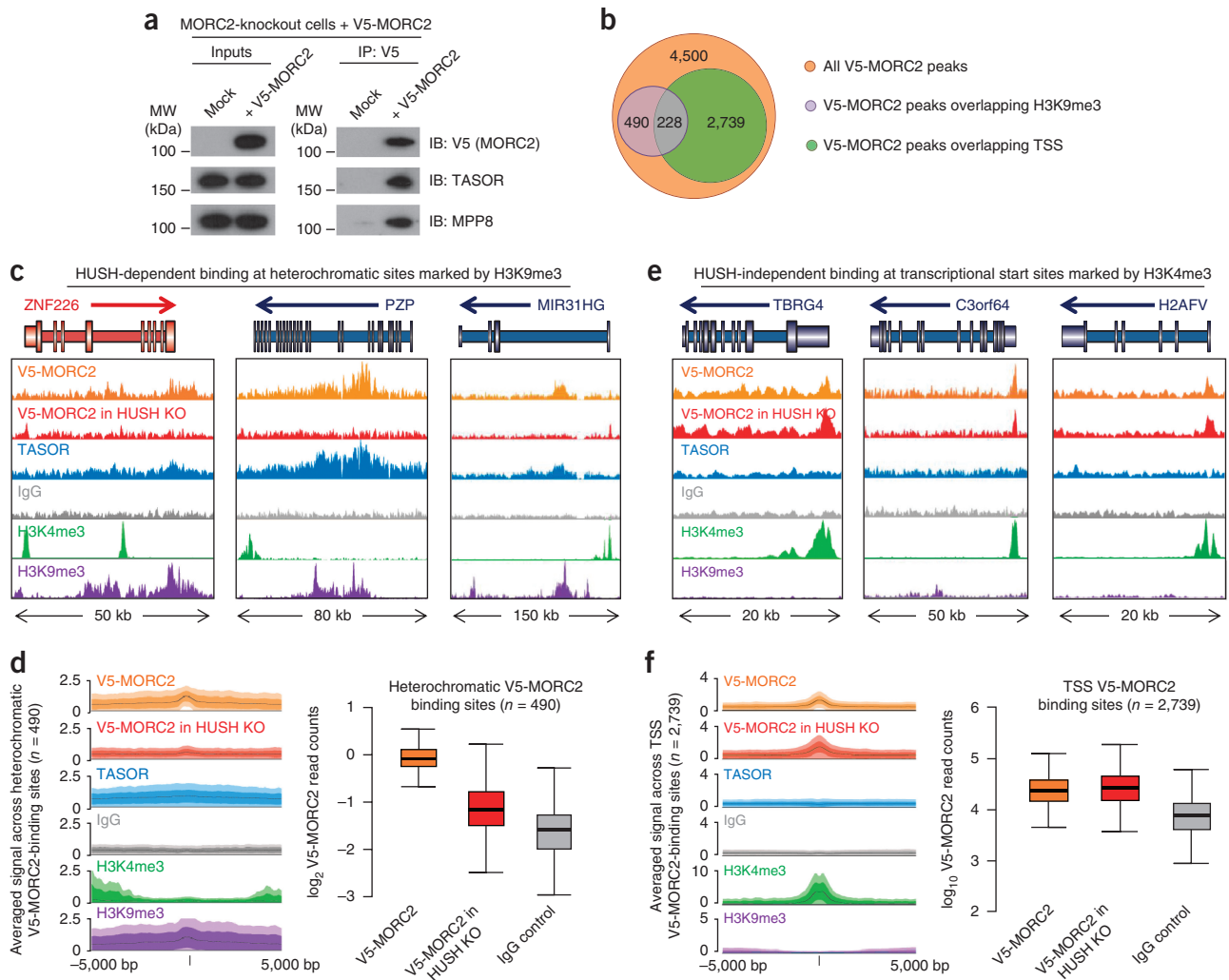


**Figure 3** The HUSH complex recruits MORC2 to heterochromatic target sites. **(a)** MORC2 interacts with the HUSH complex. TASOR and MPP8 coimmunoprecipitate with V5-tagged MORC2 expressed in HeLa cells. **(b)** Summary of MORC2 genome occupancy, as measured by ChIP-seq. In total, 4,500 peaks of V5-MORC2 occupancy were detected, most of which fell into two categories: binding sites in heterochromatin marked by H3K9me3 (purple; left) and binding sites at TSSs (green; right). **(c,d)** The HUSH complex recruits MORC2 to heterochromatic sites marked by H3K9me3. TASOR and MORC2 occupancy was observed at a range of sites marked by H3K9me3; MORC2 recruitment at these sites was dependent on HUSH, as V5-MORC2 occupancy was lost in cells lacking all three HUSH subunits<sup>9</sup> (HUSH KO). Three example loci are shown in **c**, and summary data across all loci are shown in **d**. Full ChIP-seq traces including input DNA controls are shown in **Supplementary Figure 3a**. For box plots: center line, median; box limits, upper and lower quartiles; whiskers, 1.5 $\times$  interquartile range. **(e,f)** MORC2 recruitment to transcriptional start sites is independent of the HUSH complex. MORC2 occupancy was observed at a large number of TSSs marked by the H3K4me3 histone modification. This occupancy was independent of the HUSH complex, because TASOR occupancy was not observed at these sites, and MORC2 occupancy was maintained in cells lacking HUSH subunits. Three example loci are shown in **e**, and summary data across all loci are shown in **f**. Full ChIP-seq traces including input DNA controls are shown in **Supplementary Figure 3b**.

in SETDB1-knockout cells (**Supplementary Fig. 2d**), and deletion of MORC2 did not prevent the interaction between SETDB1 and HUSH (**Supplementary Fig. 2e**), thereby suggesting independent recruitment of these two potential effector proteins by the HUSH complex. However, like SETDB1, MORC2 did not appear to be a constitutive member of the HUSH complex, because, in contrast to loss of TASOR, MPP8 or Periphilin<sup>9</sup>, loss of MORC2 did not affect the protein levels of HUSH subunits (**Supplementary Fig. 2f**) or their localization to chromatin (**Supplementary Fig. 2g**).

### The HUSH complex recruits MORC2 to heterochromatic loci

To ascertain the physiological relevance of the association between MORC2 and the HUSH complex, we performed chromatin immunoprecipitation followed by deep sequencing (ChIP-seq).

Immunoprecipitation of a V5-tagged MORC2 construct expressed in MORC2-knockout cells revealed two modes of MORC2 binding to chromatin (**Fig. 3b**): a broad distribution across the bodies of genes located in H3K9me3-marked heterochromatin (**Fig. 3c,d** and **Supplementary Fig. 3a**) and a series of discrete peaks at transcription start sites (TSSs) (**Fig. 3e,f** and **Supplementary Fig. 3b**). Comparing the occupancy of MORC2 with that of endogenous TASOR revealed a substantial overlap between the heterochromatic regions bound by MORC2 and those occupied by the HUSH complex (**Fig. 3c,d**). Indeed, MORC2 localization to these heterochromatic sites was dependent on the HUSH complex, as MORC2 occupancy was lost in cells lacking all three HUSH subunits (**Fig. 3c,d**). Thus, these data sets revealed HUSH-dependent recruitment of MORC2 to heterochromatic loci marked by H3K9me3. The functional relevance of MORC2 recruitment

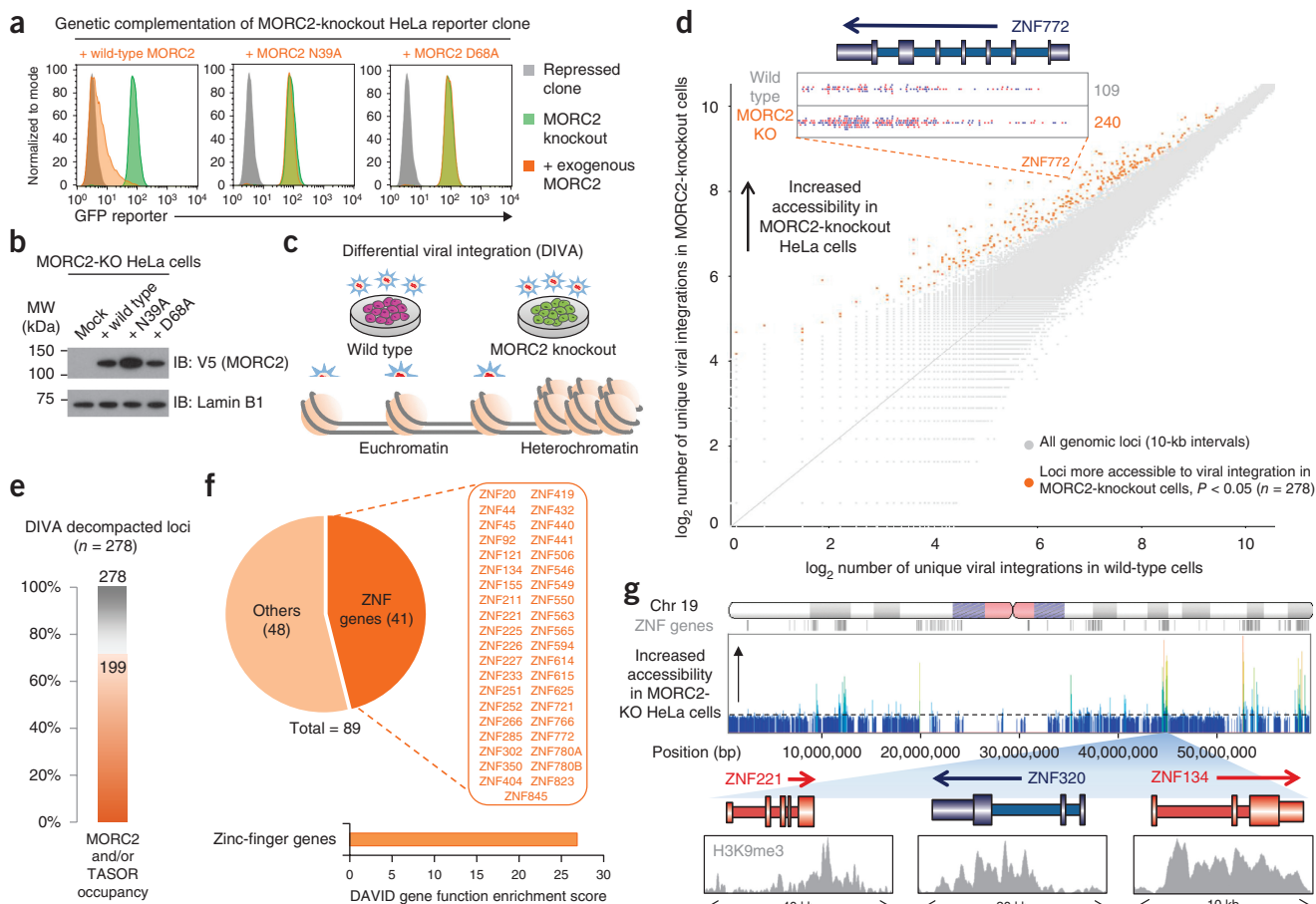


**Figure 4** Loss of MORC2 results in chromatin decompaction at HUSH-target sites. **(a,b)** ATP hydrolysis by MORC2 is critical for HUSH-mediated transgene repression. **(a)** Exogenous expression of MORC2 mutants unable to bind (p.Asn39Ala; denoted N39A) or hydrolyze (p.Asp68Ala; denoted D68A) ATP did not rescue reporter repression in MORC2-knockout cells. **(b)** Immunoblot validation of expression of the MORC2 point mutants. **(c)** Overview of the DIVA methodology, which uses large-scale mapping of lentiviral integration sites to probe accessible chromatin (additional details in **Supplementary Fig. 5c,d**). **(d)** Loss of MORC2 results in chromatin decompaction. Scatter plot highlighting the 289 genomic loci (orange) exhibiting increased accessibility in MORC2-knockout cells. Unique lentiviral integration sites mapped to the *ZNF772* locus in wild-type and MORC2-knockout cells are shown as an example. DIVA scores for all genomic loci are detailed in **Supplementary Table 2**. **(e)** Most loci exhibiting decompaction after MORC2 knockout are direct targets of MORC2 and the HUSH complex. Of the 278 decompacted loci, MORC2 and/or TASOR occupancy was detected at 199 loci (71%). **(f,g)** Loci exhibiting decompaction after MORC2 knockout are highly enriched in ZNF genes **(f)**, and the decompacted regions across chromosome 19 correspond to sites of ZNF gene clusters **(g)**. Chr, chromosome.

to TSSs remains unclear, but this recruitment was not dependent on the HUSH complex (**Fig. 3e,f**) and did not involve recognition of Lys4-trimethylated H3 (H3K4me3) by the CW domain of MORC2 (ref. 22) (**Supplementary Fig. 4**), as has been demonstrated for the CW domains of MORC3 and MORC4 (refs. 23,24).

In further support of an association between HUSH and MORC2, we also found that the HUSH complex regulated the expression of *MORC2*. Knockout of HUSH subunits or SETDB1 resulted in an increase in *MORC2* expression, as measured by quantitative reverse transcription PCR (qRT-PCR) (**Supplementary Fig. 2h**). In addition, our ChIP-seq data demonstrated both TASOR occupancy and HUSH-dependent recruitment of MORC2 to an H3K9me3-rich site in the *MORC2* promoter, thus further suggesting a direct feedback loop (**Supplementary Fig. 2i**).

### MORC2 loss results in chromatin decompaction at HUSH loci

The catalytic activity of the MORC2 ATPase domain allows MORC2 to remodel nucleosomal templates *in vitro*<sup>25</sup>. Therefore, we hypothesized that ATP hydrolysis by MORC2 might be required to alter chromatin

architecture at HUSH-target sites *in vivo*. To directly test the functional requirement for MORC2 ATPase activity in HUSH-mediated silencing, we carried out further genetic complementation assays in MORC2-knockout HeLa cells (**Fig. 4a**). Whereas exogenous expression of wild-type MORC2 restored HUSH function and resulted in the rerepression of the GFP reporter construct, MORC2 variants bearing point substitutions in the critical residues of the ATPase domain required for ATP binding (p.Asn39Ala) or hydrolysis (p.Asp68Ala)<sup>25</sup> were nonfunctional (**Fig. 4a,b**).

If the ATPase activity of MORC2 were required to mediate chromatin compaction during HUSH-mediated repression *in vivo*, disruption of *MORC2* would result in a more open chromatin structure at sites of HUSH activity. Assay for transposase-accessible chromatin with high-throughput sequencing (ATAC-seq) is currently a leading method to assay changes in chromatin accessibility *in vivo*<sup>26</sup>, but our attempts to exploit this technology to examine potential chromatin decompaction in MORC2-knockout HeLa cells were hampered by a large proportion of contaminating mitochondrial reads<sup>27</sup> and insufficient coverage of the heterochromatic portions of the genome at which

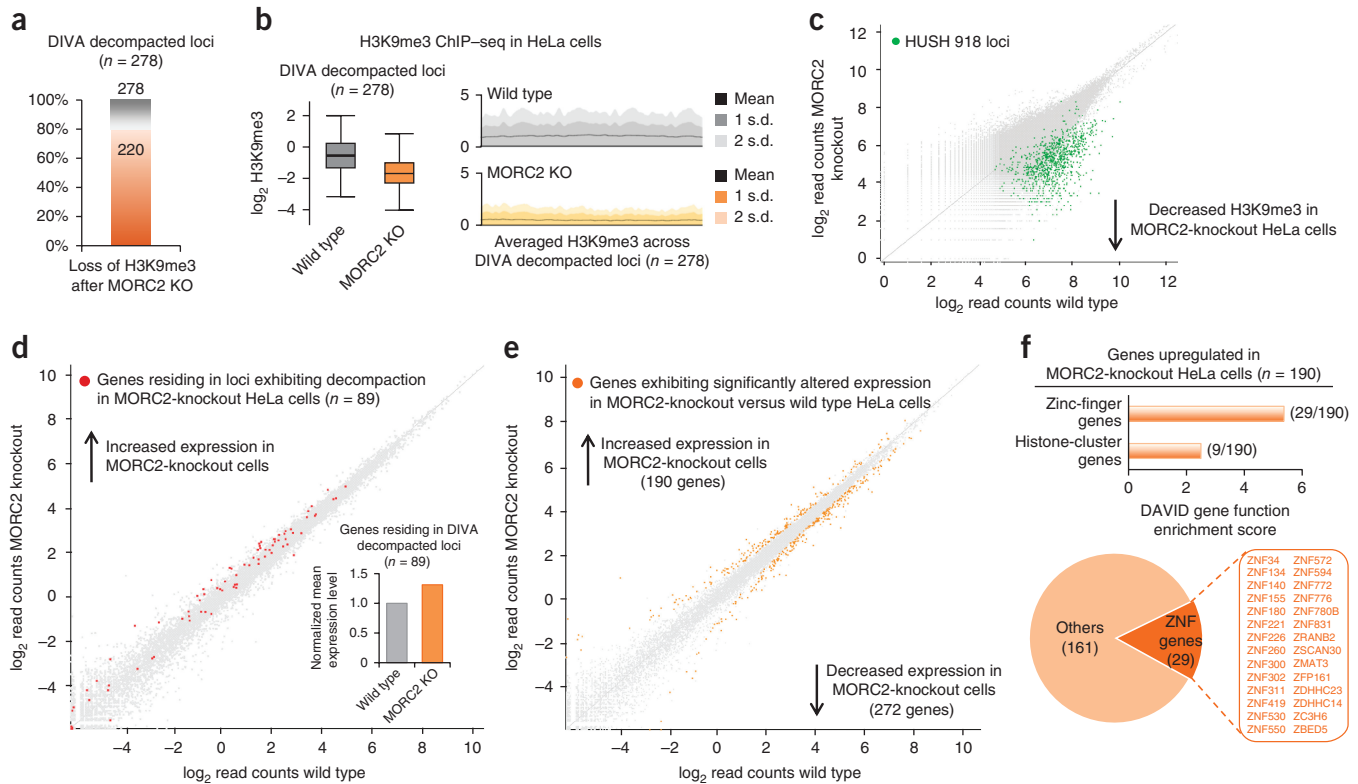


**Figure 5** Chromatin decompaction in MORC2-knockout cells is accompanied by a loss of H3K9me3 and transcriptional depression. **(a,b)** H3K9me3 is lost across most loci exhibiting decompaction after MORC2 knockout. **(a)** Of the 278 decompacted loci, a loss of H3K9me3 after MORC2 knockout in HeLa cells was observed at 220 loci (79%), as measured by ChIP-seq. **(b)** Summary data across all 278 decompacted loci. **(c)** Knockout of MORC2 results in loss of H3K9me3 at the same sites that lose H3K9me3 after knockout of HUSH subunits. Previously, in HeLa cells, we identified 918 genomic loci that lost H3K9me3 after knockout of either TASOR, MPP8 or Periphilin (green dots)<sup>9</sup>; these same loci also exhibited decreased H3K9me3 levels after knockout of MORC2. **(d,e)** The effect of MORC2 knockout on the transcriptome. RNA-seq analysis was performed to compare the transcriptomes of wild-type and MORC2-knockout HeLa cells. In **d**, genes residing in loci exhibiting decompaction in MORC2-knockout cells ( $n = 89$ ) are highlighted in red; loci exhibiting decompaction also exhibit increased expression, as measured by RNA-seq (inset). In **e**, all genes exhibiting significantly altered expression between wild-type and MORC2-knockout cells ( $n = 462$ ; DEseq  $P < 0.05$ ) are highlighted in orange. **(f)** Functional classification of the genes upregulated in MORC2-knockout cells through the DAVID functional annotation tool. Genes upregulated after MORC2 knockout are highly enriched in ZNF genes.

HUSH functions (Supplementary Fig. 5a,b). We therefore developed a new approach, differential viral accessibility (DIVA), to examine changes in chromatin accessibility *in vivo*. DIVA is conceptually similar to ATAC-seq, but, rather than identifying transposon integration sites to probe accessible chromatin, DIVA maps the integration sites of exogenous lentiviruses (Fig. 4c and Supplementary Fig. 5c). In contrast to the Tn5 transposase, which preferentially integrates near TSSs, HIV-1-derived lentiviral vectors preferentially target gene bodies<sup>28</sup>.

We used DIVA to compare chromatin accessibility in wild-type and MORC2-null HeLa cells. Approximately 20 million independent viral integration sites were mapped in each cell type, and the two data sets were then compared to identify loci exhibiting significantly greater numbers of integrations in the MORC2-knockout cells compared with the parental wild-type cells (Fig. 4c and Supplementary Fig. 5d–g). Considering the genome as a series of 10-kb windows, we identified 278 loci exhibiting chromatin decompaction after knockout of MORC2 (Fig. 4d and Supplementary Table 2). A large proportion of these loci were heterochromatic sites at which TASOR or MORC2 occupancy was observed by ChIP-seq (Fig. 4e). Notably, many of these loci contained genes encoding zinc-finger (ZNF) proteins (ZNF genes; Fig. 4f); for example, on chromosome 19, which is rich in ZNF genes, a striking

concordance was observed between the positions of clusters of ZNF genes and the loci exhibiting decompaction in MORC2-knockout cells (Fig. 4g). Using an orthogonal technique based on micrococcal nuclease sensitivity, we validated increased chromatin accessibility in MORC2-knockout cells at four example loci containing ZNF genes (Supplementary Fig. 6).

### MORC2 loss results in decreased H3K9me3 and transcriptional derepression

We also sought to assess the relationship between MORC2-dependent changes in chromatin accessibility and H3K9me3 deposition. We found that loss of MORC2 in HeLa cells resulted in a decrease in H3K9me3 at most loci exhibiting chromatin decompaction after MORC2 knockout (Fig. 5a,b and Supplementary Fig. 7a), thus supporting the idea that chromatin decompaction results in a concomitant decrease in H3K9me3 levels. In agreement with the functional association between MORC2 and the HUSH complex, 906 of the 918 loci (99%) that we previously found to lose H3K9me3 after deletion of any of the three HUSH subunits<sup>9</sup> also showed decreased H3K9me3 levels in MORC2-knockout cells (Fig. 5c). At most of these sites, H3K9me3 deposition was dependent on the HUSH-associated methyltransferase SETDB1 (Supplementary Fig. 7a,b).

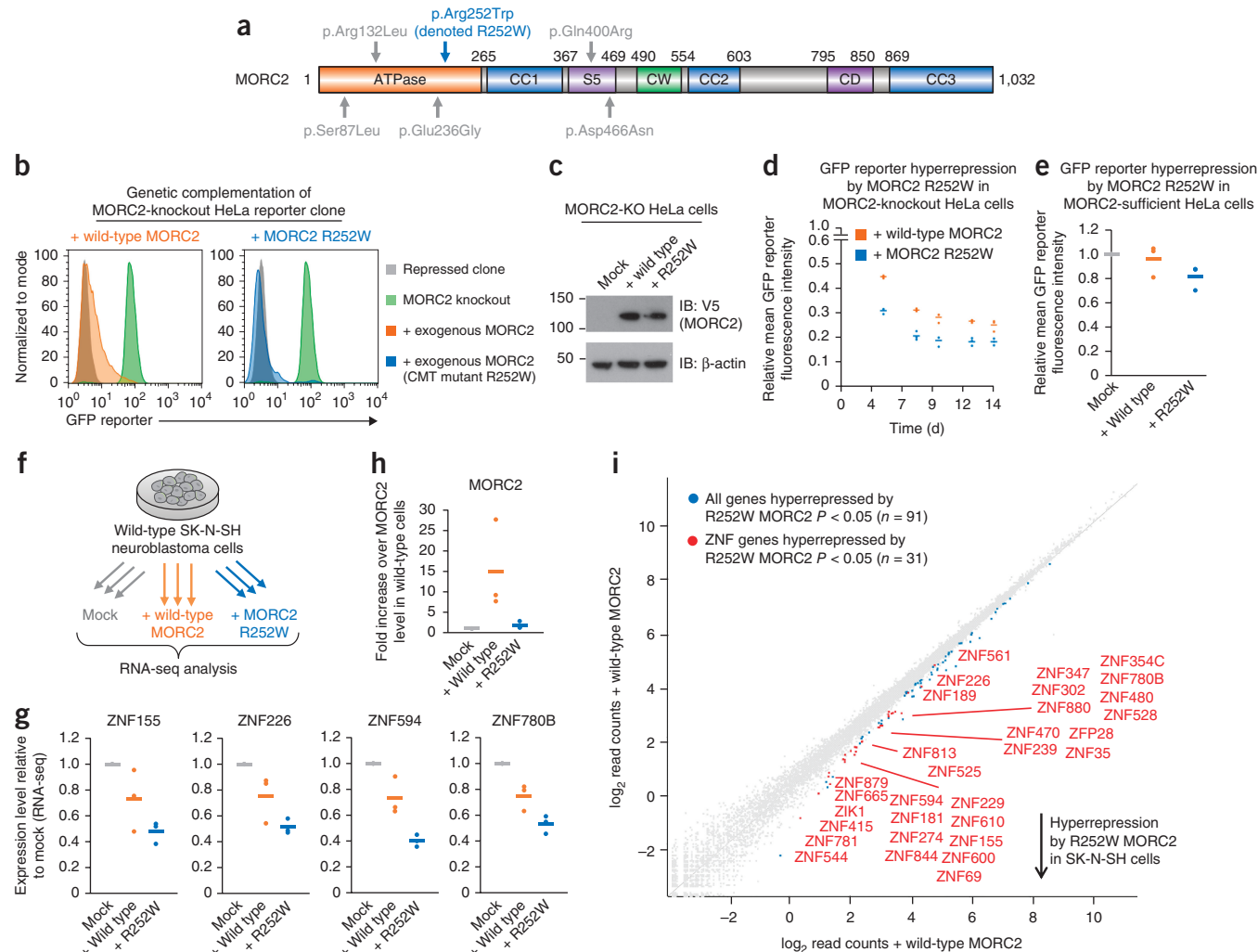


**Figure 6** The p.Arg252Trp alteration in MORC2, which is associated with CMT disease, hyperactivates HUSH-mediated epigenetic repression. **(a)** Schematic representation of the alterations associated with CMT affecting the ATPase domain of MORC2. **(b,c)** Assessing the effect of the p.Arg252Trp CMT alteration on MORC2 function through genetic complementation of MORC2-knockout cells. **(b)** The p.Arg252Trp (denoted R252W) CMT-mutant MORC2 is functional, restoring HUSH-mediated transgene silencing when expressed in MORC2-knockout cells. **(c)** Immunoblot validation of expression of wild-type or p.Arg252Trp-mutant MORC2. **(d,e)** The p.Arg252Trp CMT alteration in MORC2 hyperactivates HUSH-mediated transgene silencing in HeLa cells. **(d)** Time course of transgene rerepression in MORC2-knockout HeLa cells. The p.Arg252Trp MORC2 mutant increases both the rate and overall extent of transgene rerepression. **(e)** Hyper-repression of a GFP<sup>dim</sup> HUSH reporter in MORC2-sufficient cells by overexpression of p.Arg252Trp MORC2. **(f)** Schematic representation of the RNA-seq experiment in wild-type SK-N-SH neuroblastoma cells. **(g-i)** Expression of either wild-type MORC2 or the p.Arg252Trp mutant results in hyper-repression of HUSH-target genes. **(g)** RNA-seq in SK-N-SH cells overexpressing either wild-type or p.Arg252Trp MORC2 reveals hyper-repression of example HUSH-target genes. **(h)** Despite p.Arg252Trp MORC2 being expressed at a much lower level than the wild-type protein, this effect was more pronounced with the p.Arg252Trp mutant. **(i)** In total, 91 genes were hyper-repressed by the p.Arg252Trp mutant (edgeR  $P < 0.05$ ), of which 31 were ZNF genes.

Finally, we considered the effect of chromatin decompaction at these sites on gene expression. In addition to a decrease in H3K9me<sub>3</sub>, we found that decompaction after knockout of MORC2 resulted in an increase in the mean expression level of the 89 genes within these loci (Fig. 5d), with 42 genes (47%) displaying a >1.2-fold increase in expression. Furthermore, of all the 190 genes significantly upregulated after MORC2 knockout (Fig. 5e), ZNF genes were the most significantly enriched functional group (Fig. 5f). In agreement with a repressive role for MORC2, most of the upregulated genes were direct targets of TASOR and/or MORC2, (Supplementary Fig. 7c,d), and many also exhibited a loss of H3K9me<sub>3</sub> and decompaction after MORC2 knockout (Supplementary Fig. 7e). In contrast, ablation of MORC2 did not result in a global transcriptional change across genes

exhibiting HUSH-independent MORC2 occupancy at their TSSs (Supplementary Fig. 7f). Altogether, these data support a model in which loss of MORC2 results in chromatin decompaction, a loss of SETDB1-mediated H3K9me<sub>3</sub> deposition and transcriptional derepression at HUSH-target sites.

#### p.Arg252Trp CMT substitution in MORC2 hyperactivates HUSH silencing

Five independent studies have recently reported that dominant mutations in the sequence encoding the ATPase domain of MORC2 can cause axonal CMT disease<sup>29–33</sup> (Fig. 6a). We focused on understanding the functional effects of the most prevalent alteration, which results in an arginine-to-tryptophan substitution at residue

252 (p.Arg252Trp in UniProt Q9Y6X9-1) and causes a severe axonal form of CMT2 (ref. 30). This substitution is identical to the previously reported p.Arg190Trp variant of MORC2 (refs. 29,31,32), which refers to a putative alternative isoform of the protein (UniProt Q9Y6X9-2) that lacks 62 amino acids at the N terminus.

In agreement with the genetic data suggesting a gain-of-function mechanism underlying the pathogenicity of the mutations, MORC2 with the p.Arg252Trp substitution did encode a functional protein capable of restoring HUSH-mediated transgene repression in MORC2-knockout HeLa cells (Fig. 6b,c). Moreover, the p.Arg252Trp mutant consistently outperformed the wild-type protein, thus resulting in enhanced rerepression of the GFP reporter. Indeed, despite being expressed at a lower level than the wild-type protein, the p.Arg252Trp substitution both accelerated the rate of reporter rerepression and enhanced the overall degree of reporter repression observed (Fig. 6d and Supplementary Fig. 8). To verify that this effect was also present at endogenous genes targeted by HUSH and MORC2, we performed RNA-seq analysis to compare the transcriptome of MORC2-knockout HeLa cells reconstituted with wild-type MORC2 with that of the p.Arg252Trp mutant (Supplementary Fig. 9). In agreement with the results from the reporter assays, we found that the p.Arg252Trp substitution resulted in the hyper-repression of MORC2-target genes (Supplementary Fig. 9).

The mutant MORC2 proteins exert a dominant effect in CMT patients, driving the disease phenotype when coexpressed with a wild-type MORC2 allele. Therefore, we considered whether the p.Arg252Trp mutant MORC2 could hyper-repress HUSH-target genes when it was expressed together with the wild-type protein in MORC2-sufficient cells. First, we found that overexpression of p.Arg252Trp MORC2, but not wild type, resulted in hyper-repression of a HUSH-responsive 'GFP<sup>dim</sup>' HeLa reporter clone that exhibited weak expression at steady state (Fig. 6e). We then considered whether this effect might also occur at endogenous genes in neuronal cells. Transcriptome analysis of SK-N-SH neuroblastoma cells by RNA-seq (Fig. 6f) showed that overexpression of either wild-type or p.Arg252Trp MORC2 enhanced repression at example HUSH-target sites (Fig. 6g); however, this effect was substantially greater with the p.Arg252Trp mutant, although it was expressed at ~7.5-fold lower levels than the wild-type protein (Fig. 6h). Indeed, of the 91 genes significantly overrepressed by p.Arg252Trp protein compared with the wild-type protein, 31 (34%) were ZNF genes marked by H3K9me3 (Fig. 6i). Overall, these data suggested that the p.Arg252Trp substitution in MORC2 hyperactivates HUSH-mediated epigenetic repression, thus resulting in over-repression of HUSH-target genes in neuronal cells.

## DISCUSSION

The recently identified HUSH complex is an important regulator of mammalian heterochromatin that is critical for silencing of newly integrated retroviruses<sup>9</sup> and for normal embryonic development<sup>12,13</sup>. Here, through a genome-wide CRISPR-Cas9-mediated forward genetic screen, we identified MORC2 as an additional accessory member of the HUSH complex. MORC2 is recruited by the HUSH complex to heterochromatic loci, where its ATPase activity is essential for HUSH-mediated silencing. Exploiting a new method, DIVA, we found that loss of MORC2 resulted in chromatin decompaction at these sites, which was accompanied by a decrease in H3K9me3 levels and transcriptional derepression. Furthermore, we found that the most commonly identified CMT disease alteration in the MORC2 ATPase domain, p.Arg252Trp, resulted in hyperactivation of HUSH-mediated repression at heterochromatic loci.

Previously we identified the HUSH complex through a gene-trap mutagenesis screen in the near-haploid KBM7 human cell line<sup>9</sup>. The

rapid emergence of CRISPR-Cas9-mediated genome editing technologies allowed us to reexamine the complement of genes required for transgene repression, using a genome-wide library of sgRNAs to create the starting pool of mutant cells. The results of the two screens proved to be complementary, because, although the CRISPR screen did not identify two of the core HUSH complex subunits detected by the original haploid gene-trap screen, it did reveal an essential role of one additional gene, MORC2 (Fig. 1). The CRISPR screening technique is therefore a powerful alternative to the haploid gene-trap approach<sup>14</sup>, and, given the considerable interest in designing more efficacious guide RNA libraries<sup>34-36</sup>, it is likely that the accuracy of such genome-wide CRISPR screens will continue to improve.

In humans, the MORC protein family comprises four proteins (MORC1-4) plus the more divergent SMCHD1 (ref. 19). MORC1 represses transposable elements in the male mouse germ line<sup>21</sup>, and MORC2 has been implicated in the response to DNA damage<sup>25</sup>, but the molecular function of the mammalian MORC family members remains largely uncharacterized. All MORC proteins share a similar domain architecture comprising an N-terminal GHKL-type ATPase domain and a CW-type zinc-finger, but their functions are likely to be distinct. For example, the inability of the CW-type zinc-fingers of MORC1 and MORC2 to recognize methylated H3K4 suggests a different mode of recruitment to chromatin compared with those of MORC3 and MORC4 (ref. 22), whereas only alterations in MORC2 are associated with CMT disease<sup>29-33</sup>. A key challenge, therefore, is to elucidate how MORC proteins are recruited to chromatin and to determine their effects on nucleosomal architecture at target sites. Here, we found that HUSH regulates the localization of MORC2 to target sites on chromatin, and that the ATPase activity of MORC2 plays a critical role in altering chromatin architecture at these sites during HUSH-mediated silencing.

The ATPase activity of MORC2 is required to drive nucleosome remodeling *in vitro*<sup>25</sup>; furthermore, we found this activity to be essential for transgene silencing by the HUSH complex *in vivo* (Fig. 4a,b). Therefore, it followed that the remodeling activity of MORC2 might be required to alter chromatin architecture at these sites and consequently promote gene silencing. Although ATAC-seq has been widely used to study the degree of chromatin 'opening' at TSSs, we found it unsuitable to probe decompaction of heterochromatic regions, owing to the low proportion of transposon integrations into such sites. Instead of mapping transposon integration sites, DIVA examines the integration preferences of exogenous lentiviruses to probe accessible chromatin. Lentiviruses preferentially target the bodies of genes<sup>28</sup>, and indeed our data showed that this approach affords far greater coverage of the heterochromatic sites at which the HUSH complex functions. We therefore anticipate that DIVA may prove to be a useful approach to interrogate changes in heterochromatin structure *in vivo* in other experimental systems. However DIVA may not be suitable for comparisons between nonisogenic cell lines, because it may be impossible to control for differences in the abundance or activity of other factors influencing viral integration preferences. Furthermore DIVA relies on high-efficiency transduction with lentiviral vectors, which may not be achievable in all cell types, and, in contrast to the simplicity of ATAC-seq, requires a more involved protocol for the preparation of sequencing libraries to map virus-genome junctions.

Our application of DIVA to compare wild-type and MORC2-null cells revealed that loss of MORC2 resulted in chromatin decompaction at HUSH-target sites. The repetitive ZNF gene family was the most enriched functional group. Many of the ZNF genes are located in clusters covered by high levels of H3K9me3, a mark also found in other repetitive regions of the genome, including centromeres

and tandem repeats. Although we did not observe decompaction of these additional repetitive regions after MORC2 disruption, we do not know how well DIVA might capture these other sites of repressive heterochromatin. Further experiments will be needed to address the specific physiological role of MORC2 with HUSH and SETDB1 in maintaining H3K9me3 across the bodies of ZNF-encoding genes.

The DIVA results suggested that HUSH-target loci normally adopt a compact chromatin state, which must be reversed to alleviate repression. Although repressed genomic regions have canonically been associated with dense chromatin domains that are refractory to the transcription machinery, there may be distinct mechanisms through which such nucleosome compaction is achieved. In particular, the specific requirement for ATP hydrolysis to drive compaction during HUSH-mediated silencing appears to be distinct from the requirements of other key repressive complexes. For example, ATP hydrolysis has not been implicated in heterochromatin formation through the SUV39H1–HP1 axis, another major route to H3K9me3-mediated silencing. Compact heterochromatic structures have also been associated with Polycomb-driven repression<sup>37</sup>, but again this compaction function does not appear to require an ATP motor and has instead been attributed to a disordered region rich in basic amino acids in PRC1 (ref. 38). However, ATP-dependent chromatin remodelers have previously been shown to play an indirect role in transcriptional repression by establishing the appropriate nucleosome spacing for subsequent silencing<sup>39</sup>. For example, the nucleosome remodeling deacetylase (NuRD) complex utilizes the chromatin remodeling function of its CHD subunits to space adjacent nucleosomes, thereby making the histone tails accessible for deacetylation<sup>40</sup>. Therefore, one possibility is that MORC2 may be recruited by HUSH and consequently position nucleosomes such that the chromatin is permissive to transcriptional repression.

The mechanism through which dominant mutations in *MORC2* cause axonal CMT disease<sup>29–33</sup> and severe spinal muscular atrophy (SMA)-like disease<sup>41</sup> is unknown. Given that individuals with this disease retain one functional wild-type *MORC2* allele, the disease phenotype is unlikely to result from loss of function of the mutant protein. Our data suggested that a gain-of-function effect underlies the phenotype of the *MORC2* p.Arg252Trp CMT substitution and results in hyperactivation of HUSH complex function at both exogenous transgenes and endogenous genomic loci. Indeed, the closely related MORC1 protein, which represses transposable elements in the male germ line<sup>21</sup>, contains a tryptophan residue at the equivalent position.

Further work will be required to elucidate the biochemical basis underlying the hyperactivation phenotype resulting from the *MORC2* p.Arg252Trp substitution. Structural insight into the organization of the *MORC2* ATPase domain would be invaluable in assessing the effects of the p.Arg252Trp substitution and may also guide the rational design of small-molecule inhibitors. Inhibition of Hsp90, the prototypical member of the GHKL family of ATPases, has been successfully achieved by using the small molecules geldanamycin and radicicol<sup>42,43</sup>, and the latter is also effective against the distantly related GHKL family member SMCHD1 (ref. 44). Overall, these data suggest that inhibition of the ATPase domain of *MORC2* is an attractive target for the therapeutic modulation of HUSH complex function.

## METHODS

Methods, including statements of data availability and any associated accession codes and references, are available in the [online version of the paper](#).

*Note: Any Supplementary Information and Source Data files are available in the online version of the paper.*

## ACKNOWLEDGMENTS

We are indebted to CIMR core facilities: R. Schulte and his team for FACS, and M. Gratian and M. Bowen for microscopy. We thank S. Andrews for assistance with data analysis with SeqMonk, and S. Kundu and M. Tolstorukov for helpful discussions. We thank B. Cochran (Tufts University), F. Radow (MRC-LMB), D. Rubinsztein (CIMR) and M. Brenner (Harvard Medical School) for providing materials. This work was supported by the Wellcome Trust, through a Principal Research Fellowship to P.J.L. (101835/Z/13/Z), a Senior Research Fellowship to Y.M. (101908/Z/13/Z), a Sir Henry Wellcome Postdoctoral Fellowship to R.T.T. (201387/Z/16/Z) and a PhD studentship to I.A.T., and by the BBSRC, through a Future Leader Fellowship to C.H.D. I.A.T. is supported as a Damon Runyon Fellow by the Damon Runyon Cancer Research Foundation (DRG-2277-16). The CIMR is in receipt of a Wellcome Trust strategic award.

## AUTHOR CONTRIBUTIONS

I.A.T., R.T.T. and P.J.L. conceived the study. Except for the *in vitro* expression and purification experiments, which were carried out by C.H.D., I.A.T. and R.T.T. performed all of the experiments and, together with Y.M. and P.J.L., analyzed the data and wrote the manuscript. G.D., R.C.R. and R.E.K. contributed essential reagents.

## COMPETING FINANCIAL INTERESTS

The authors declare no competing financial interests.

Reprints and permissions information is available online at <http://www.nature.com/reprints/index.html>. Publisher's note: Springer Nature remains neutral with regard to jurisdictional claims in published maps and institutional affiliations.

- Wang, J., Lawry, S.T., Cohen, A.L. & Jia, S. Chromosome boundary elements and regulation of heterochromatin spreading. *Cell. Mol. Life Sci.* **71**, 4841–4852 (2014).
- Margueron, R. & Reinberg, D. The Polycomb complex PRC2 and its mark in life. *Nature* **469**, 343–349 (2011).
- Becker, J.S., Nicetto, D. & Zaret, K.S. H3K9me3-dependent heterochromatin: barrier to cell fate changes. *Trends Genet.* **32**, 29–41 (2016).
- Talbert, P.B. & Henikoff, S. Spreading of silent chromatin: inaction at a distance. *Nat. Rev. Genet.* **7**, 793–803 (2006).
- Schotta, G., Ebert, A., Dorn, R. & Reuter, G. Position-effect variegation and the genetic dissection of chromatin regulation in *Drosophila*. *Semin. Cell Dev. Biol.* **14**, 67–75 (2003).
- Akhtar, W. *et al.* Chromatin position effects assayed by thousands of reporters integrated in parallel. *Cell* **154**, 914–927 (2013).
- Kotecki, M., Reddy, P.S. & Cochran, B.H. Isolation and characterization of a near-haploid human cell line. *Exp. Cell Res.* **252**, 273–280 (1999).
- Carette, J.E. *et al.* Haploid genetic screens in human cells identify host factors used by pathogens. *Science* **326**, 1231–1235 (2009).
- Tchakovnikarova, I.A. *et al.* Epigenetic silencing by the HUSH complex mediates position-effect variegation in human cells. *Science* **348**, 1481–1485 (2015).
- Schultz, D.C., Ayyanathan, K., Negorev, D., Maul, G.G. & Rauscher, F.J. III. SETDB1: a novel KAP-1-associated histone H3, lysine 9-specific methyltransferase that contributes to HP1-mediated silencing of euchromatic genes by KRAB zinc-finger proteins. *Genes Dev.* **16**, 919–932 (2002).
- Kokura, K., Sun, L., Bedford, M.T. & Fang, J. Methyl-H3K9-binding protein MPP8 mediates E-cadherin gene silencing and promotes tumour cell motility and invasion. *EMBO J.* **29**, 3673–3687 (2010).
- Harten, S.K. *et al.* The first mouse mutants of D14Abbl1 (Fam208a) show that it is critical for early development. *Mamm. Genome* **25**, 293–303 (2014).
- Soehn, A.S. *et al.* Periphilin is strongly expressed in the murine nervous system and is indispensable for murine development. *Genesis* **47**, 697–707 (2009).
- Timms, R.T. *et al.* Genetic dissection of mammalian ERAD through comparative haploid and CRISPR forward genetic screens. *Nat. Commun.* **7**, 11786 (2016).
- Timms, R.T., Tchakovnikarova, I.A., Antrobus, R., Dougan, G. & Lehner, P.J. ATF7IP-mediated stabilization of the histone methyltransferase setdb1 is essential for heterochromatin formation by the HUSH complex. *Cell Rep.* **17**, 653–659 (2016).
- Wang, T., Wei, J.J., Sabatini, D.M. & Lander, E.S. Genetic screens in human cells using the CRISPR-Cas9 system. *Science* **343**, 80–84 (2014).
- Shalem, O. *et al.* Genome-scale CRISPR-Cas9 knockout screening in human cells. *Science* **343**, 84–87 (2014).
- Sanjana, N.E., Shalem, O. & Zhang, F. Improved vectors and genome-wide libraries for CRISPR screening. *Nat. Methods* **11**, 783–784 (2014).
- Li, D.-Q., Nair, S.S. & Kumar, R. The MORC family: new epigenetic regulators of transcription and DNA damage response. *Epigenetics* **8**, 685–693 (2013).
- Moissiard, G. *et al.* MORC family ATPases required for heterochromatin condensation and gene silencing. *Science* **336**, 1448–1451 (2012).
- Pastor, W.A. *et al.* MORC1 represses transposable elements in the mouse male germline. *Nat. Commun.* **5**, 5795 (2014).

22. Liu, Y. *et al.* Family-wide characterization of histone binding abilities of human CW domain-containing proteins. *J. Biol. Chem.* **291**, 9000–9013 (2016).
23. Liu, Y. *et al.* Structure and function of CW domain containing proteins. *Curr. Protein Pept. Sci.* **17**, 497–506 (2016).
24. Li, S. *et al.* Mouse MORC3 is a GHKL ATPase that localizes to H3K4me3 marked chromatin. *Proc. Natl. Acad. Sci. USA* **113**, E5108–E5116 (2016).
25. Li, D.-Q. *et al.* MORC2 signaling integrates phosphorylation-dependent, ATPase-coupled chromatin remodeling during the DNA damage response. *Cell Rep.* **2**, 1657–1669 (2012).
26. Buenrostro, J.D., Giresi, P.G., Zaba, L.C., Chang, H.Y. & Greenleaf, W.J. Transposition of native chromatin for fast and sensitive epigenomic profiling of open chromatin, DNA-binding proteins and nucleosome position. *Nat. Methods* **10**, 1213–1218 (2013).
27. Wu, J. *et al.* The landscape of accessible chromatin in mammalian preimplantation embryos. *Nature* **534**, 652–657 (2016).
28. Kvaratskhelia, M., Sharma, A., Larue, R.C., Serrao, E. & Engelman, A. Molecular mechanisms of retroviral integration site selection. *Nucleic Acids Res.* **42**, 10209–10225 (2014).
29. Sevilla, T. *et al.* Mutations in the MORC2 gene cause axonal Charcot-Marie-Tooth disease. *Brain* **139**, 62–72 (2016).
30. Albulym, O.M. *et al.* MORC2 mutations cause axonal Charcot-Marie-Tooth disease with pyramidal signs. *Ann. Neurol.* **79**, 419–427 (2016).
31. Laššuthová, P. *et al.* Severe axonal Charcot-Marie-Tooth disease with proximal weakness caused by de novo mutation in the MORC2 gene. *Brain* **139**, e26 (2016).
32. Hyun, Y.S., Hong, Y.B., Choi, B.O. & Chung, K.W. Clinico-genetics in Korean Charcot-Marie-Tooth disease type 2Z with MORC2 mutations. *Brain* **139**, e40 (2016).
33. Zhao, X. *et al.* MORC2 mutations in a cohort of Chinese patients with Charcot-Marie-Tooth disease type 2. *Brain* **139**, e56 (2016).
34. Wang, T. *et al.* Identification and characterization of essential genes in the human genome. *Science* **350**, 1096–1101 (2015).
35. Doench, J.G. *et al.* Optimized sgRNA design to maximize activity and minimize off-target effects of CRISPR-Cas9. *Nat. Biotechnol.* **34**, 184–191 (2016).
36. Horlbeck, M.A. *et al.* Compact and highly active next-generation libraries for CRISPR-mediated gene repression and activation. *eLife* **5**, e19760 (2016).
37. Francis, N.J., Kingston, R.E. & Woodcock, C.L. Chromatin compaction by a polycomb group protein complex. *Science* **306**, 1574–1577 (2004).
38. Grau, D.J. *et al.* Compaction of chromatin by diverse Polycomb group proteins requires localized regions of high charge. *Genes Dev.* **25**, 2210–2221 (2011).
39. Clapier, C.R. & Cairns, B.R. The biology of chromatin remodeling complexes. *Annu. Rev. Biochem.* **78**, 273–304 (2009).
40. Zhang, Y., LeRoy, G., Seelig, H.P., Lane, W.S. & Reinberg, D. The dermatomyositis-specific autoantigen Mi2 is a component of a complex containing histone deacetylase and nucleosome remodeling activities. *Cell* **95**, 279–289 (1998).
41. Schottmann, G., Wagner, C., Seifert, F., Stenzel, W. & Schuelke, M. MORC2 mutation causes severe spinal muscular atrophy-phenotype, cerebellar atrophy, and diaphragmatic paralysis. *Brain* **139**, e70 (2016).
42. Stebbins, C.E. *et al.* Crystal structure of an Hsp90-geldanamycin complex: targeting of a protein chaperone by an antitumor agent. *Cell* **89**, 239–250 (1997).
43. Sharma, S.V., Agatsuma, T. & Nakano, H. Targeting of the protein chaperone, HSP90, by the transformation suppressing agent, radicicol. *Oncogene* **16**, 2639–2645 (1998).
44. Chen, K. *et al.* Genome-wide binding and mechanistic analyses of Smc1-mediated epigenetic regulation. *Proc. Natl. Acad. Sci. USA* **112**, E3535–E3544 (2015).

## ONLINE METHODS

**Cell culture.** HeLa cells were obtained from ECACC and were grown in RPMI 1640 plus 10% FCS and penicillin/streptomycin (100 U/ml); the approximate doubling time was 22–23 h for both wild-type cells and all derivative cell lines. KBM7 cells, obtained from B. Cochran<sup>7</sup>, and HEK 293ET cells, a gift from F. Randow, were cultured in IMDM plus 10% FCS and penicillin/streptomycin (100 U/ml). SK-N-SH cells, a gift from D. Rubinsztein, were grown in DMEM plus 10% FCS and penicillin/streptomycin (100 U/ml); the approximate doubling time was 55–60 h for both wild-type cells and all derivative cell lines. All cell lines were routinely tested for mycoplasma contamination with an ATCC Universal Mycoplasma Detection Kit.

**Antibodies.** The following primary antibodies were used: rabbit anti-MORC2 (Bethyl Laboratories, A300-149A used for immunoblotting), rabbit anti-MORC2 (Santa Cruz Biotechnology, sc-366271, used for immunofluorescence), rabbit anti-TASOR (Atlas Antibodies, HPA006735), rabbit anti-MPP8 (Proteintech, 16796-1-AP), rabbit anti-SETDB1 (Proteintech, 11231-1-AP), mouse anti-GFP (Life Technologies, A11120), mouse anti-V5 (Abcam, ab27671), rabbit anti-V5 (Abcam, ab15828), goat anti-Lamin B1 (Santa Cruz, sc-6217), rabbit anti-H3K9me3 (Abcam, ab8898), rabbit anti-histone H3 (Biolegend, 601902), rabbit IgG (Cell Signaling, 2729), mouse anti-calnexin (AF8, a kind gift from M. Brenner) and mouse anti- $\beta$ -actin (Sigma-Aldrich, A5316). Alexa Fluor 488- and Alexa Fluor 546-conjugated secondary antibodies for immunofluorescence were obtained from Molecular Probes (A32723 and A-11010). HRP-conjugated secondary antibodies for immunoblotting were obtained from Jackson ImmunoResearch (715-035-150 and 711-035-152). Validation information is available on the manufacturers' websites.

**CRISPR-Cas9-mediated forward genetic screen.** Previously, we have generated a polyclonal population of GFP<sup>dim</sup> KBM7 cells bearing epigenetically repressed transgenes through lentiviral transduction with a vector expressing a GFP-fusion protein from the SFFV LTR promoter (pHRSIN-P<sub>SFFV</sub>-GFP-HLA-A2). The Cas9 nuclease was stably expressed in this population through lentiviral transduction and subsequent hygromycin selection (500  $\mu$ g/ml). One hundred million Cas9-expressing reporter KBM7 cells were transduced with the GeCKO v2 sgRNA library at a multiplicity of infection of ~0.1, and untransduced cells were removed from the population through puromycin selection (0.75  $\mu$ g/ml) commencing 48 h after transduction. GFP<sup>bright</sup> cells resulting from the mutagenesis were enriched by two rounds of FACS, with the first sort taking place 7 d after mutagenesis and the second sort taking place an additional 7 d later. Genomic DNA was extracted (Gentra Puregene Kit) from the selected GFP<sup>bright</sup> cells after the second sort, together with a representative sample of the unsorted mutagenized library that had been grown in parallel for the equivalent amount of time.

The abundance of sgRNAs in each sample was quantified by Illumina sequencing. The variable region of the sgRNAs was amplified in a nested PCR reaction (Q5 High-Fidelity Polymerase, NEB) with forward primers binding the U6 promoter region and reverse primers binding the constant region of the sgRNA. For PCR 1, 32 100- $\mu$ l reactions, each with 4  $\mu$ g of DNA were performed for the unselected library sample, and 32 100- $\mu$ l reactions, each with 4  $\mu$ g of DNA were performed for selected cell samples. The products of these reactions were pooled, one-tenth was purified with Agencourt AMPure XP beads (Beckman Coulter), and one-tenth of the resulting DNA was used as a template for 12 cycles of PCR 2 with Illumina P5- and P7-adapted primers. After further AMPure XP bead purification, PCR products were quantified, pooled and sequenced on an Illumina HiSeq 2500 instrument with 50-bp single-end reads from a custom primer binding immediately upstream of the sgRNA sequence. All primer sequences are detailed in **Supplementary Table 3**.

The resulting sequence reads were trimmed of the constant portion of the sgRNA with the fastx toolkit and then aligned to an index of the GeCKO v2 library with Bowtie 2. Uniquely aligning reads were used to generate sgRNA-count tables for each sample, which were analyzed further with the RSA algorithm to identify genes significantly enriched in gene-disruption events in the selected cells compared with the unselected library.

**Individual CRISPR-Cas9-mediated gene disruption.** Oligonucleotides (Sigma-Aldrich) for top and bottom strands of the sgRNA were phosphorylated

with T4 PNK (NEB), annealed by heating to 95 °C and subsequent slow cooling to room temperature, and then cloned into either the dual Cas9/sgRNA expression vector pSpCas9(BB)-2A-Puro (Addgene 48139, kindly deposited by F. Zhang<sup>45</sup>) or the lentiviral sgRNA expression vector pKLV-U6gRNA(BbsI)-PGKpuro2ABFP (Addgene 50946, kindly deposited by K. Yusa<sup>46</sup>).

**Lentiviral expression.** Exogenous gene expression was achieved with the expression vectors pHRSIN-P<sub>SFFV</sub>-GFP-P<sub>PGK</sub>-Hygro, pHRSIN-P<sub>SFFV</sub>-GFP-IRES-mCherry-P<sub>PGK</sub>-Hygro and pHRSIN-P<sub>SFFV</sub>-GFP-P<sub>PGK</sub>-Blasto, with the gene of interest inserted in place of GFP. For lentiviral expression of shRNA constructs, the pHR-SIREN vector was used with hairpins cloned in as BamHI-EcoRI fragments. In all cases, lentivirus particles were generated through the triple transfection of HEK 293ET cells with the lentiviral transfer vector plus the two packaging plasmids pCMV $\Delta$ R8.91 and pMD.G, by using TransIT-293 transfection reagent (Mirus) according to the manufacturer's recommendations. Viral supernatant was typically harvested 48 h after transfection, cell debris was removed with a 0.45- $\mu$ m filter, and target cells were transduced by spin infection at 800g for 60 min. Transduced HeLa cells were selected with the following drug concentrations: puromycin, 2  $\mu$ g/ml; hygromycin, 50  $\mu$ g/ml; and blasticidin, 3  $\mu$ g/ml. Transduced SK-N-SH cells were selected with 50  $\mu$ g/ml hygromycin.

**Flow cytometry.** Cells were fixed in 1% PFA and analyzed on a FACSCalibur (BD) or a FACSFortessa (BD) instrument. Data were analyzed with FlowJo software. For cell sorting, cells were resuspended in PBS with 2% FCS, and FACS was carried out on an Influx cell sorter (BD).

**Immunofluorescence.** HeLa cells were grown overnight on glass coverslips, fixed with 4% PFA for 10 min, permeabilized with 0.5% Triton X-100 for 5 min, and then blocked for at least 30 min with 4% BSA dissolved in PBS and 0.1% Tween-20 (PBS-T). The primary antibody was diluted in 40  $\mu$ l of blocking solution and was applied for 1 h, and, after five washes in PBS-T, fluorophore-conjugated secondary antibody (Molecular Probes) was applied for 45 min in the same manner. After an additional five washes in PBS-T and a final rinse in distilled water, coverslips were mounted in 4  $\mu$ l ProLong Gold Antifade Mountant with DAPI (Thermo Fisher Scientific) and imaged with a Nikon LSM880 laser scanning confocal microscope (Zeiss). Images were processed with Adobe Photoshop or GIMP 2.

**Coimmunoprecipitation.** Cells were washed once in PBS and then lysed in cell lysis buffer (0.5% IGEPAL, 85 mM KCl and 10 mM HEPES in distilled water). Nuclei were harvested by centrifugation at 800g for 5 min at 4 °C and then lysed in nuclear lysis buffer (1% IGEPAL plus 1:100 benzonase in TBS). Insoluble nuclear material was removed by centrifugation (10,000g for 5 min at 4 °C), and then the supernatant was precleared with protein G magnetic beads (Thermo Fisher Scientific) for 1 h at 4 °C. Immunoprecipitation was performed by addition of 1  $\mu$ g of antibody and protein G magnetic beads for 2 h at 4 °C. The beads were then washed three times in lysis buffer, and samples were eluted in SDS sample buffer.

**Immunoblotting.** Cells were lysed in 1% SDS with 1:100 benzonase (Sigma-Aldrich) for 20 min at room temperature and then heated to 70 °C in SDS sample buffer for 10 min. After separation by SDS-PAGE, proteins were transferred to a PVDF membrane (Millipore), which was then blocked in 5% milk in PBS and 0.2% Tween-20. Membranes were probed overnight with the indicated antibodies, washed three times with PBS and 0.2% Tween-20, and then incubated with HRP-conjugated secondary antibodies (Jackson ImmunoResearch) for 45 min at room temperature. Reactive bands were visualized with SuperSignal West Pico or West Dura (Thermo Fisher Scientific) reagents. All blots presented in the figures have been cropped; the original uncropped images can be found in **Supplementary Figure 10**.

**Subcellular fractionation.** One million cells were washed in PBS and then again in buffer A (10 mM HEPES, 1.5 mM MgCl<sub>2</sub>, 10 mM KCl, 0.5 mM DTT and an EDTA-free protease-inhibitor-cocktail tablet (Roche)). The cells were then lysed after resuspension in buffer A with 0.1% (vol/vol) IGEPAL on ice for 10 min. Nuclei were pelleted by centrifugation (1,400g for 4 min at 4 °C),

and the supernatant, which contained the cytosolic fraction, was collected. The nuclear pellet was resuspended in buffer B (20 mM HEPES, 1.5 mM MgCl<sub>2</sub>, 300 mM NaCl, 0.5 mM DTT, 25% (vol/vol) glycerol, 0.2 mM EDTA and an EDTA-free protease-inhibitor-cocktail tablet) for 10 min on ice, and after centrifugation at 1,700g for 4 min at 4 °C, the supernatant (containing the nucleosolic fraction) was removed. The insoluble pellet, constituting the chromatin fraction, was subsequently solubilized in 1% SDS with 1:100 benz-onase for 20 min at room temperature.

**ChIP-seq.** Cells were washed once in PBS, resuspended in growth medium and then cross-linked in 1% formaldehyde for 10 min. The reaction was quenched for 5 min by addition of glycine to a final concentration of 0.125 M, and the cells were lysed in cell lysis solution (1 mM HEPES, 85 mM KCl and 0.5% IGEPAL). Nuclei were pelleted by centrifugation and then resuspended in nuclear lysis solution (5 mM Tris, 10 mM EDTA and 1% SDS) for 10 min. The chromatin was sheared with a Bioruptor (Diagenode; high power, 20 cycles of 30 s on and 30 s off) to obtain a mean fragment size of ~300 bp. Insoluble material was removed by centrifugation. The chromatin solution was precleared with Protein A–Sepharose (Sigma–Aldrich) and then immunoprecipitated overnight with 5 µg primary antibody and Protein A–Sepharose, or, for V5-MORC2, anti-V5 agarose affinity gel (Sigma–Aldrich, A7345). The next day, the beads were washed five times, and bound protein–DNA complexes were eluted in 150 mM NaHCO<sub>3</sub> and 1% SDS. Cross-links were reversed by overnight incubation at 67 °C with 0.3 M NaCl and RNase A. Proteinase K was then added, the samples were incubated for 2 h at 45 °C, and then the DNA was purified with a spin column (Qiagen PCR Purification Kit). Illumina sequencing libraries were produced from this material with a TruSeq ChIP Sample Prep Kit (Illumina), and 50-bp single-end reads were generated on a HiSeq 2500 instrument. Reads were aligned to the human genome (GRCh37) with Bowtie 2, and reads with a MAPQ score >10 were imported into SeqMonk and EaSeq<sup>47</sup> for further analysis. V5-MORC2-binding sites were identified through implementation of the MACS peak caller in SeqMonk (window size, 300 bp; *P* value <0.0001), and the resulting 4,500 peaks were centered and plotted with the Average Signal Tracks tool in EaSeq. H3K4me3 ChIP-seq data generated by the laboratory of B. Bernstein (Broad Institute) were downloaded from the ENCODE project (ENCSR000AOF).

**qRT-PCR.** RNA was prepared with an RNeasy Plus kit (Qiagen) and converted into cDNA with Super RT reverse transcriptase (HT Biotechnology) and a poly(dT) primer. Quantification by qPCR was performed on an ABI 7500 Real Time PCR System (Applied Biosystems) with SYBR green PCR Master Mix (Life Technologies) in a final reaction volume of 25 µl. The thermal cycling parameters were: 50 °C for 2 min; 95 °C for 5 min; 40 cycles of 95 °C for 15 s; and 58 °C for 1 min. Error bars represent the s.d. of at least three technical replicates. Primer sequences are provided in **Supplementary Table 3**.

**Expression and purification of the CW domain of MORC2.** A synthetic *Escherichia coli* codon-optimized DNA construct (IDT) encoding the MORC2 CW domain (residues 490–546) plus a C-terminal FLAG tag was cloned into the expression vector pET-28a-N-His-SUMO between the BamHI and NotI restriction sites, for production of the N-terminally histidine-SUMO-tagged protein product. Protein was produced in *E. coli* BL21(DE3) cells through overnight incubation at 18 °C with shaking at 220 r.p.m., after induction with 200 µM IPTG. Cell pellets were resuspended in 30 ml lysis buffer (50 mM Tris-HCl, 500 mM NaCl, 10 mM imidazole, 0.1 mM ZnSO<sub>4</sub>, 1 mM DTT and 1× Complete EDTA-free protease inhibitors, pH 8.0), flash frozen in liquid nitrogen and stored at –80 °C.

Pellets were thawed and further lysed by sonication on ice before clarification by centrifugation (45 min, 40,000g, 4 °C). The resulting histidine-SUMO-CW-FLAG-containing supernatant was subjected to immobilized Ni–NTA affinity chromatography with wash (50 mM Tris-HCl, 500 mM NaCl, 10 mM imidazole, 0.1 mM ZnSO<sub>4</sub> and 1 mM DTT, pH 8.0) and elution (50 mM Tris-HCl, 500 mM NaCl, 300 mM imidazole, 0.1 mM ZnSO<sub>4</sub> and 1 mM DTT, pH 8.0) buffers, then desalted with a Bio-Rad Econo-Pac 10DG column into cleavage buffer (20 mM HEPES, 150 mM NaCl, 0.1 mM ZnSO<sub>4</sub> and 1 mM DTT, pH 7.4). The histidine-SUMO tag was cleaved from the protein by the addition of histidine-tagged SENP1 protease (1:10 (wt/wt) for 18 h on ice. Subtractive

immobilized Ni–NTA affinity chromatography was then used to deplete the tagged protease and the free histidine-SUMO tag, and the protein was further purified by size-exclusion chromatography on a Superdex 75 (10/300) column in a buffer containing 20 mM HEPES, 200 mM NaCl, 0.1 mM ZnSO<sub>4</sub> and 1 mM TCEP, pH 7.3. The masses of the intact, pure proteins were confirmed with a Waters Xevo G2 Q-ToF mass spectrometer.

**Differential viral accessibility (DIVA).** Six million wild-type and MORC2-knockout HeLa cells were seeded at a density of 1 × 10<sup>6</sup> cells per well of a six-well plate and transduced on successive days with the lentiviral vector pHR SIN-P<sub>SPFV</sub>-mCherry-WPRE (encoding the mCherry fluorescent protein driven by the spleen focus-forming virus LTR promoter) at a high multiplicity of infection, such that ~100% of the cells were positive for mCherry. One day after the second transduction, genomic DNA was extracted (Gentra Puregene Kit) and digested overnight with NlaIII (NEB). The distribution of NlaIII sites in the lentiviral vector was such that DNA fragments smaller than ~1.8 kb could not contain viral-genome junctions; large fragments were therefore enriched through a size-selection step with a 0.5× Agencourt AMPure XP bead clean-up (Beckman Coulter). An annealed dsDNA adaptor with an NlaIII-compatible overhang was then ligated onto the ends of the genomic DNA fragments with T4 DNA Ligase (NEB) overnight at 16 °C, and the ligated products were purified through further AMPure bead cleanup. Virus-genome junctions were then amplified in 200 cycles of a linear PCR reaction with Accuprime Taq (Thermo Fisher Scientific) with a biotinylated primer binding immediately upstream of the 5′ LTR in the integrated provirus, and the resulting products were annealed to streptavidin-coated M-280 Dynabeads (Thermo Fisher Scientific). After five 10-min washes with PBS and 0.1% Tween-20, virus-genome junctions were amplified through 12 cycles of on-bead exponential PCR with an Illumina P5-adapted primer binding the proviral 5′ LTR and a P7-adapted reverse primer binding the splinkerette adaptor. After a final AMPure XP cleanup, PCR products were quantified, pooled and sequenced on an Illumina HiSeq2500 instrument generating 50-bp single-end reads from a custom primer annealing to the extreme end of the proviral 5′ LTR. All oligonucleotide sequences are detailed in **Supplementary Table 3**.

The resulting sequence reads were trimmed of adaptor sequences with the fastx toolkit and aligned to the human genome (hg19) with Bowtie 2. Reads with a MAPQ score >10 were imported into SeqMonk and converted into a set of unique points of integration. The Intensity Difference Filter in Seqmonk was used to identify 10-kb genomic windows (overlapping by 5 kb) significantly enriched in lentiviral integration sites in MORC2-knockout cells compared with the parental wild-type cells; individual loci were considered to exhibit decompaction only if at least two adjacent windows reached statistical significance. Full data for all genomic loci are provided in **Supplementary Table 2**.

**Micrococcal nuclease accessibility assay.** Wild-type and MORC2-knockout HeLa cells were washed once in PBS, resuspended in growth medium, and then cross-linked by the addition of 1% formaldehyde for 10 min. The reaction was quenched by addition of glycine to a final concentration of 0.125 M for 5 min. The cells were then lysed in cell lysis solution (1 mM HEPES, 85 mM KCl and 0.5% IGEPAL), and nuclei were pelleted by centrifugation (800g, 5 min, 4 °C). The nuclei (5 × 10<sup>5</sup> per reaction) were then resuspended in micrococcal nuclease buffer supplemented with BSA (NEB), and chromatin was digested by the addition of 2 U micrococcal nuclease (NEB) for 30 min at 37 °C. EDTA was added to a final concentration of 45 mM to stop the reaction. Nuclei were then lysed in 1% SDS, RNA was digested with RNase A (37 °C for 30 min), and cross-links were reversed overnight at 65 °C. Proteins were then digested with proteinase K (37 °C for 2 h), and DNA was isolated by phenol–chloroform extraction and subsequent ethanol precipitation. Size selection of the digested DNA was achieved with SPRIselect beads (Beckman Coulter) with a 0.6× volume of beads. The bound fraction contained large fragments (>~1,000 bp); the supernatant containing unbound fragments (<~1,000 bp) was removed and subsequently purified through the addition of an additional 1× volume of beads. The amount of DNA from target loci in the accessible and inaccessible fractions compared with the pre-size-selected starting material was measured by qPCR performed on a CFX96 Touch Real-Time PCR machine (Bio-Rad) with iTaq Universal SYBR Green Supermix (Bio-Rad) in a final reaction volume of 25 µl. Thermal cycling parameters were 50 °C for

2 min; 95 °C for 5 min; 40 cycles of 95 °C for 15 s and 58 °C for 1 min. Error bars represent the s.d. of at least three technical replicates. Primer sequences are shown in **Supplementary Table 3**.

**RNA-seq.** Total RNA was extracted with an miRNEasy kit (Qiagen), per the manufacturer's instructions, and multiplexed Illumina sequencing libraries were prepared with a TruSeq Stranded Total RNA Library Prep Kit (Illumina). For the comparison between wild-type and MORC2-knockout HeLa cells, ribosomal RNA was depleted with a Ribo-Zero Gold rRNA Removal Kit (Epicentre), and 150-bp paired-end reads were generated on an Illumina HiSeq2500 instrument. For all comparisons between wild-type and p.Arg252Trp MORC2, poly(A)<sup>+</sup> RNA was sequenced on an Illumina HiSeq2500 instrument with 50-bp single-end reads. Sequence reads were aligned to the human genome (GRCh37) with HISAT2. Mapped reads with a MAPQ score >40 were imported into SeqMonk and further analyzed with the RNA-seq quantification pipeline and subsequent DEseq2 or edgeR analysis.

**Statistics.** No statistical methods were used to predetermine sample size. Experiments were not randomized, and the experimenters were not blinded to outcomes. Genes significantly enriched in inactivating mutations in the CRISPR screen were evaluated with the RSA algorithm comparing the frequency of sgRNAs in the GFP<sup>bright</sup>-selected population and the unselected mutagenized pool. All qRT-PCR data are represented as the mean ± s.d. of

at least three technical replicates, and the data are representative of at least two independent experiments. For the RNA-seq data presented in **Figure 5e**, three independent MORC2-knockout clones were used; genes exhibiting significantly altered expression in MORC2-knockout cells were identified through DEseq2 in Seqmonk ( $P < 0.05$ ). For the RNA-seq data presented in **Figure 6g–i**, cells were transduced in triplicate with lentiviral vectors to express either wild-type or p.Arg252Trp-mutant MORC2; genes exhibiting significantly decreased expression after expression of the p.Arg252Trp mutant as compared with wild-type MORC2 were identified through implementation of edgeR in Seqmonk ( $P < 0.05$ ).

**Data availability.** The sequence data from the CRISPR–Cas9 forward genetic screen, ChIP–seq, DIVA and RNA-seq experiments that support the findings of this study have been deposited in the Gene Expression Omnibus database under primary accession code [GSE95480](https://www.ncbi.nlm.nih.gov/geo/query/acc.cgi?acc=GSE95480).

45. Ran, F.A. *et al.* Genome engineering using the CRISPR-Cas9 system. *Nat. Protoc.* **8**, 2281–2308 (2013).
46. Koike-Yusa, H., Li, Y., Tan, E.-P., Velasco-Herrera, Mdel.C. & Yusa, K. Genome-wide recessive genetic screening in mammalian cells with a lentiviral CRISPR-guide RNA library. *Nat. Biotechnol.* **32**, 267–273 (2014).
47. Lerdrup, M., Johansen, J.V., Agrawal-Singh, S. & Hansen, K. An interactive environment for agile analysis and visualization of ChIP-sequencing data. *Nat. Struct. Mol. Biol.* **23**, 349–357 (2016).